Controlling Short- and Long-Range Electron Transfer Processes in Molecular Dyads and Triads

Luis Sánchez,[a] Ignacio Pérez,[a] Nazario Martín,*[a] and Dirk M. Guldi*[b]

Dedicated to Professor Klaus-Dieter Asmus on the occasion of his 65th birthday

Abstract: Novel π-extended tetrathiafulvalene (exTTF)-based donor acceptor hybrids—dyads and triads—have been synthesized following a multistep synthetic procedure. Cyclic voltammetry and absorption spectroscopy, conducted in room temperature solutions, reveal features that are identical to the sum of the separate donor and acceptor moieties. Steady-state and time-resolved photolytic techniques confirm that upon photoexcitation of the fullerene chromophore, rapid ($1.25 \times 10^{10}\ s^{-1}$) and efficient (67%) charge separation leads to long-lived, charge-separated radical pairs. Typical lifetimes for the dyad ensembles range between 54 and 460 ns, with the longer values found in more polar solvents. This indicates that the dynamics are located in the 'normal region' of the Marcus curve. In the triads, subsequent charge shifts transform the adjacent radical pair into the distant radical pair, for which we determined lifetimes of up to 111 μs in DMF—values never previously accomplished in molecular triads. In the final charge-separated state, large donor-acceptor separation (center-to-center distances: ≈30 Å) minimizes the coupling between reduced acceptor and oxidized donor. Analysis of the charge recombination kinetics shows that a stepwise mechanism accounts for the unusually long lifetimes.

Keywords: charge separation · cycloaddition · donor–acceptor systems · sulfur heterocycles

Introduction

Owing to the importance and complexity of the natural photosynthetic apparatus, the study thereof requires the use of suitably simple models. Therefore, the design and synthesis of molecular architectures—artificial photosynthetic antenna and reaction centers—emerges as an interdisciplinary strategy for devising integrated, multicomponent model systems that transmit and process solar energy.[1]

Among the many photo- and redox-active donor and/or acceptor building blocks explored to construct artificial photosynthetic models,[2–5] C_{60} carries great potential as a three-dimensional, spherical electron acceptor. This is because of the small reorganization energy of C_{60} in electron transfer reactions[6] and its remarkable chemical reactivity.[7] Thus, C_{60} renders itself an excellent candidate for the preparation of photo- and redox-active systems.[8]

The continuing quest for new donor-acceptor ensembles is driven by several goals, namely faster and more efficient charge separation, slower charge recombination, minimizing the loss of excited state energy, and exploring simpler systems with fewer components.

So far, porphyrins represent the most frequently used excited state donor in combination with C_{60} (see, as a representative example, dyad **1**), generating large and complex, yet highly ordered, molecular and supramolecular

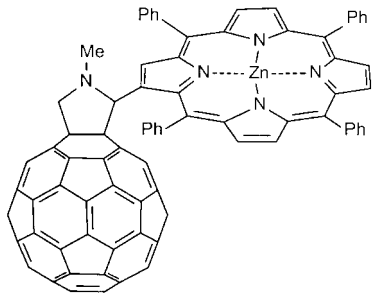

1

entities with specific functions. At small donor–acceptor separations, however, relatively short lifetimes have been reported for radical ion pairs that fall within the picosecond time scale. Longer lifetimes have been accomplished upon increasing the relative separation. To cite an instance when

[a] Prof. Dr. N. Martín, Dr. L. Sánchez, Lcdo. I. Pérez
Departamento de Química Orgánica I
Facultad de Química, Universidad Complutense, 28040 Madrid (Spain)
E-mail: nazmar@quim.ucm.es

[b] Dr. habil. D. M. Guldi
Radiation Laboratory
University of Notre Dame, Indiana 46556 (USA)
E-mail: guldi.1@nd.edu

Supporting information for this article is avalaible on the WWW under http://www.chemeurj.org or from the authors.

 DOI: 10.1002/chem.200204494

larger spacers (i.e., non photo- and electroactive moieties) were used to link donor and acceptor, lifetimes of several hundreds of nanoseconds have been recorded.

A viable alternative implies the incorporation of additional donor moieties, forming triads/tetrads/etc. The basic notion is to achieve long-distance charge-separated states using a sequence of several short-range electron transfer reactions along a well-designed redox gradient. Spectacular radical pair lifetimes—close to seconds—have been found.[6c]

The mechanism of charge recombination has a considerable impact on the rate constant. In principle, either a stepwise, that is, overcoming a thermally activated barrier (i.e., bona fide intermediate state), or a concerted pathway, that is, electronic tunneling by means of super exchange (i.e., virtual intermediate state) can occur.[9] Two factors control/alter the mechanism: 1) energy gap and 2) electronic coupling element. Importantly, slower recombination rates are expected for the stepwise scenario.

Recent reports indicate that aromatization of an oxidized donor moiety can also have a notable impact on the improvement of light-induced charge-separation.[10] An illustration is given in the case where a tetrathiafulvalene (TTF) donor has been attached in close proximity to C_{60}.[11] In the resulting C_{60}-TTF dyads (**2**, **3**), charge-separated radical ion pairs are formed whose lifetimes are in the nanosecond range. Clearly, the gain of aromaticity of the 1,3-dithiolium cation generated upon oxidation is central to this effect.

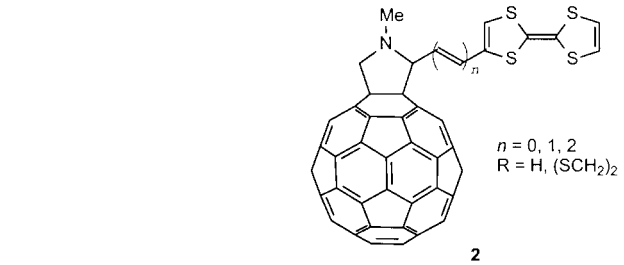

2

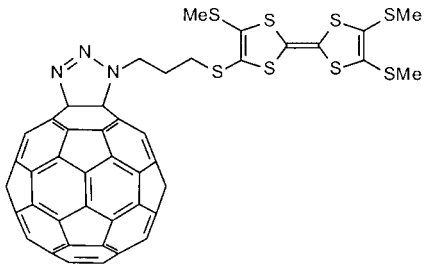

3

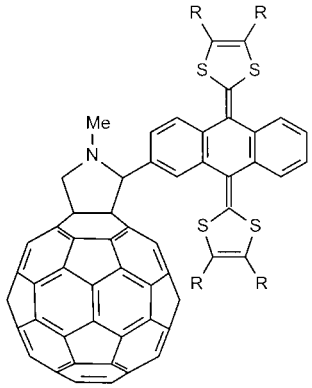

4a: R = H,
4b: R = SMe
4c: R = $(SCH_2)_2$

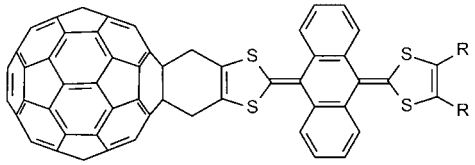

5a: R = H
5b: R = SMe

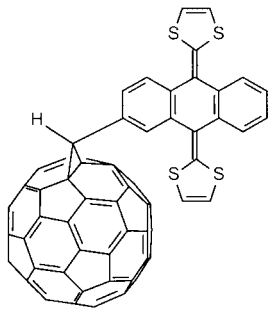

6a: R = H
6b: R = SMe

A further advance in the stabilization concept were based on the use of π-extended tetrathiafulvalenes (exTTF).[12] We have previously reported the synthesis of different C_{60}-exTTF dyads (**4**–**6**).[13] Pico- and nanosecond transient absorption measurements reveal that the instantaneously formed fullerene singlet excited state transforms rapidly into the charge-separated radical pair. Remarkably, the lifetimes of the charge-separated states in C_{60}-exTTF are in the range of several hundreds of nanoseconds in deoxygenated benzonitrile and slightly lower in the less polar CH_2Cl_2.[13c] For comparison, the parent TTF dyads (**2**) or zinc tetraphenylporphyrin dyads (**1**) yielded radical pairs having lifetimes of up to a few nanoseconds.

Herein we apply the concept of gain of aromaticity and planarity upon oxidation of the exTTF donor to a newly

Abstract in Spanish: *Nuevos sistemas dador-aceptor -díadas y tríadas- derivados de tetratíafulvaleno π-extendido (exTTF) han sido obtenidos mediante un procedimiento sintético en varios pasos. La voltamperometría cíclica y espectroscopia de absorción, realizadas en disoluciones a temperatura ambiente, muestran características que corresponden a la suma de ambos fragmentos dador y aceptor por separado. Las técnicas fotolíticas en estado estacionario y a tiempos definidos confirman que la fotoexcitación del cromóforo de fullereno conduce a una rápida (1.25×10^{10} s^{-1}) y eficiente (67 %) separación de carga con formación de pares radical con tiempos de vida largos. Los tiempos de vida típicos para las díadas oscilan entre 54 y 460 ns, con los valores más elevados encontrados en los disolventes más polares, indicando que la dinámica se localiza en la "región normal" de la curva de Marcus. En las tríadas, el posterior desplazamiento de carga transforma el par radical adyacente en un par radical a larga distancia, para el cual se ha determinado un tiempo de vida de 111 μs en DMF, valores estos que no habían sido alcanzados hasta ahora en tríadas moleculares. El análisis de la cinética de recombinación de carga indica que los elevados tiempos de vida serían debidos a un mecanismo por etapas.*

designed series of different exTTF-containing dyads and triads. Details on the synthetic, electrochemical, and photophysical work will be presented, highlighting the noteworthy impact that a chemical spacer [C_{60}-exTTF (**18**, **23**)], or a second exTTF unit [C_{60}-exTTF$_1$-exTTF$_2$ (**25**, **26**)], exert on the improvement of light-induced charge separation. Particular emphasis is placed on attaining incoherent sequential charge recombination by designing components that result in small driving forces. The lifetimes for intramolecular charge separation, determined in **25** and **26**, are by far the longest values ever reported in molecular triads.

Results and Discussion

Synthesis: Target molecules **18**, **23**, **25**, and **26** were prepared by a 1,3-dipolar cycloaddition to C_{60} of azomethine ylides generated in situ.[14]

The synthetic route towards dyad **18** is summarized in Scheme 1. The preparation of π-extended-TTF electron donors (**15a**, **b**) requires the previous protection of the hydroxy groups of the starting anthraflavic acid (2,6-dihydroxyanthraquinone) (**7**) in the form of bissilylated derivatives (**10**). This was carried out by the reaction of **7** with *tert*-butylchlorodiphenylsilane in the presence of imidazole. Subsequent twofold reaction of protected quinone **10** with a phosphorus-stabilized carbanion, generated under basic conditions (*n*-butyllithium), gave π-extended-TTFs **14a**, **b**. Compounds **14a**, **b** were deprotected by treatment with tetrabutylammonium fluoride to yield the respective diols **15a**, **b**, similar to that reported by Bryce and Marshallay.[15] Compounds **15a**, **b**, which were sparingly soluble in common organic solvents, reacted with two equivalents of 4-formylbenzoic acid (**16**) in the presence of dimethylaminopyridine (DMAP) and *N*,*N*′-dicyclohexylcarbodiimide (DCC), to afford diformyl-substituted donors **19a**, **b**, which were further used for the preparation of triads **25** and **26**.

To obtain dyad **18**, anthraflavic acid was monoalkylated with hexyl bromide and potassium carbonate, which yielded quinone **8**.[16] The remaining hydroxy group in **8** was protected by reaction with *tert*-butylchlorodiphenylsilane leading to compound **9**. Olefination of quinone **9** with phosphonate ester **11** and butyllithium gave **12**. Deprotection of the donor compound **12** by treatment with tetrabutylammonium fluoride gave the monohydroxy-substituted exTTF **13**. Finally, an esterification reaction of **13** with 4-formylbenzoic acid (**16**) afforded compound **17**, which then reacted by 1,3-dipolar cycloaddition with C_{60} and sarcosine to yield dyad **18** in 61% yield.

A similar synthetic strategy was chosen for the preparation of dyad **23** and also triads **25** and **26** (Scheme 2). In particular, 2-hydroxymethyl-9,10-bis(1,3-dithiol-2-ylidene)-9,10-dihydroanthracene (**20**)[17a] was converted with 4-formylbenzoic acid (**16**) in the presence of DMAP and DCC to the formyl-containing ester (**22**). Subsequent reaction with C_{60} and sarcosine (*N*-methylglicine) in refluxing toluene yielded **23** in 61% yield.

The synthetic workup enroute to triads **25** and **26** starts from 2-hydroxymethyl substituted exTTF **20**. In this case, **20** was transformed into a Wittig reagent (**21**) by treating it with triphenylphosphane hydrobromide ($PHPh_3^+Br^-$) in refluxing toluene.[17b] A Wittig olefination reaction with bisaldehydes **19a**, **b** in a 1:1 stoichiometric ratio gave bis-π-extended TTFs **24a**, **b** in moderate yields (43 and 38%, respectively). Finally, a cycloaddition reaction of the azomethyne ylides generated in situ from exTTF-exTTF-CHO (**24a**, **b**) and sarcosine to C_{60}

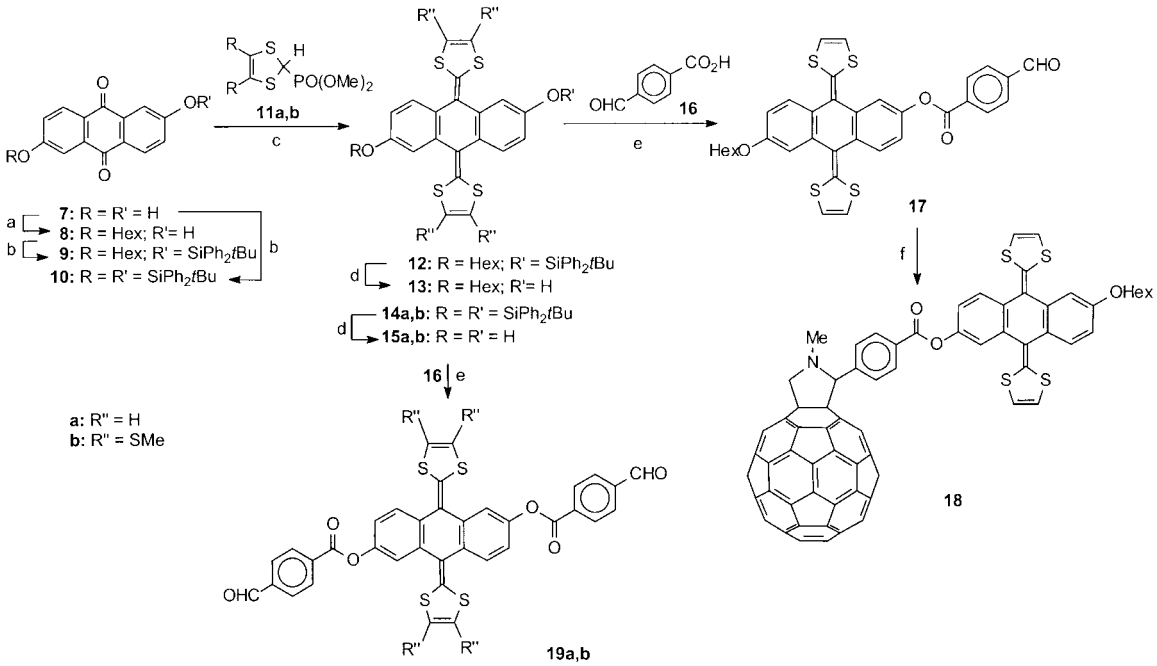

Scheme 1. a) Hexylbromide, K_2CO_3, DMF; b) tBuPh$_2$SiCl, imidazole, DMF; c) nBuLi, THF, −78 °C; d) nBu$_4$NF, THF; e) 4-carboxybenzaldehyde (**16**), DCC, DMAP, CH_2Cl_2; f) C_{60}, sarcosine, toluene, Δ.

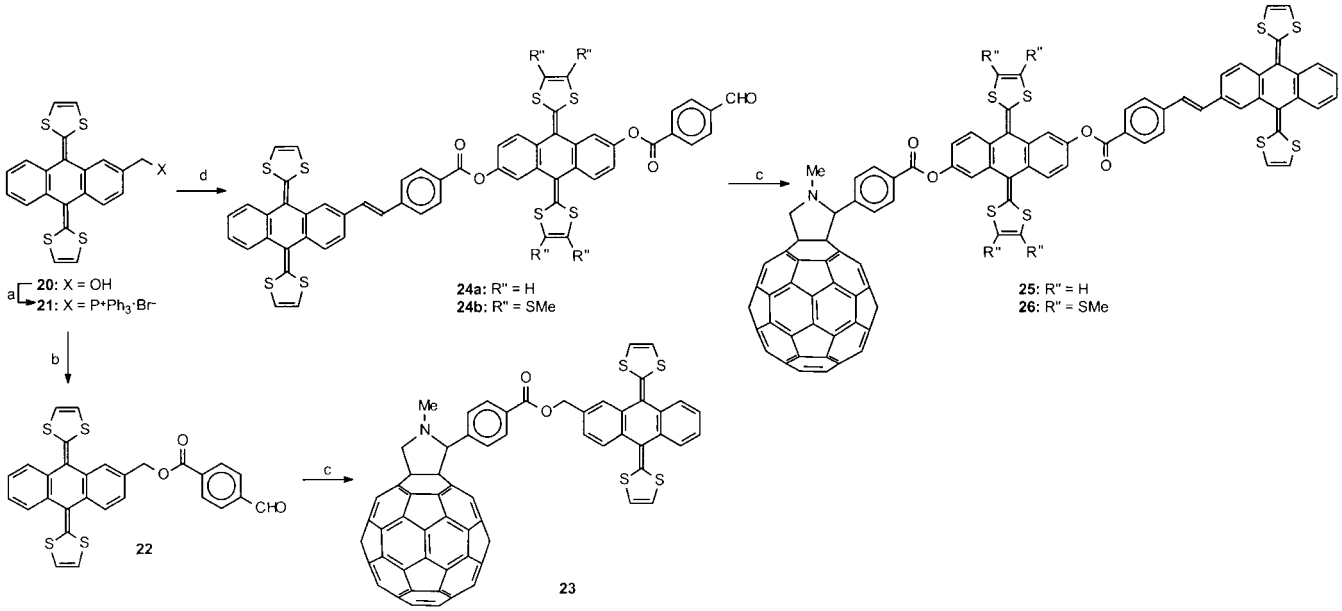

Scheme 2. a) PPh_3HBr, toluene; b) 4-carboxybenzaldehyde (**16**), DCC, DMAP, CH_2Cl_2; c) C_{60}, sarcosine, toluene, Δ d) **19a**, **b**, *t*BuOK, toluene, Δ.

yielded triads **25** and **26** as stable brown-yellowish solids in 43 and 51 % yields, respectively.

The ^{1}H NMR spectra of electroactive dyads and triads **18**, **23**, **25**, and **26** show, in addition to the aromatic signals, resonance signals of the N–Me group at $\delta = 2.9$ ppm, and the pyrrolidine protons at around $\delta = 5.01 - 5.07$ (d, $J = 9.5$ Hz, 1H), 4.30 – 4.37 (d, $J = 9.5$ Hz, 1H), and 5.01 – 5.10 ppm (s, 1H), in good agreement with other *N*-methylfulleropyrrolidine derivatives.[14] A restricted rotation of phenyl substituents on the pyrrolidine ring has been described for different phenylfulleropyrrolidine derivatives.[18] We have also observed this dynamic effect in the dyads and triads prepared, which showed broad signals for the *ortho* aromatic protons close to the fullerene surface at $\delta = 8.0$ ppm.

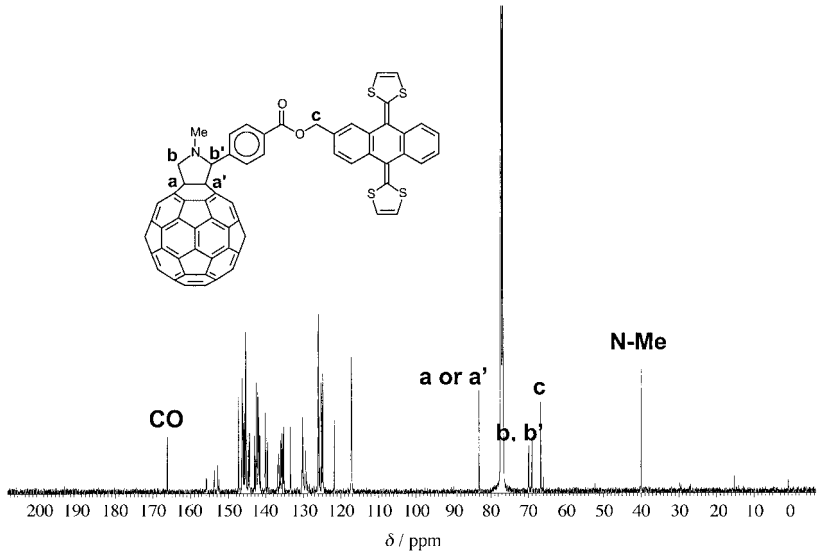

Figure 1. ^{13}C NMR spectrum for dyad **23** in $CDCl_3$.

The large number of ^{13}C NMR signals seen in $CDCl_3$:CS_2 mixtures confirm the lack of symmetry in these fulleropyrrolidine derivatives—see Experimental Section and Figure 1.

The UV/Vis spectra of **18**, **23**, **25**, and **26** show absorption bands at approximately 432 nm, which clearly correspond to the features of π-extended TTF.[12] This absorption hides the typically weak absorption band of fullerene derivatives close to 430 nm, and is responsible for the yellow color that these dyads and triads show in solution.

Electrochemistry: The CV data of the studied compounds are collected in Table 1 along with those of C_{60} and the parent unsubstituted 9,10-bis(1,3-dithiol-2-ylidene)-9,10-dihydroanthracene (**27**).[12]

Table 1. Redox potentials of **4a**, **18**, **19a**, **19b**, **22**, **23**, **25**, **26**, and **27** at room temperature.[a]

Compound	E^1_{red}	E^2_{red}	E^3_{red}	E^4_{red}	E_{ox}
4a	– 0.66	– 1.01	– 1.67	– 1.96	0.46 (2e$^-$)
18	– 0.70	– 1.08	– 1.62	– 2.01	0.41 (2e$^-$)
19a	– 1.51[b]	–	–	–	0.47 (0.45)[c] (2e$^-$)
19b	– 1.43[b]	–	–	–	0.58 (0.56)[c] (2e$^-$)
22	–	–	–	–	0.46 (2e$^-$)
23	– 0.69	– 1.07	– 1.61	– 2.01	0.39 (2e$^-$)
25	– 0.70	– 1.08	– 1.61	– 2.01	0.41 (br) (4e$^-$)
26	– 0.69	– 1.07	– 1.61	– 1.99	0.43 (br) (4e$^-$)
C_{60}	– 0.60	– 1.00	– 1.52	– 2.04	–
27[d]	–	–	–	–	0.45 (2e$^-$)

[a] Experimental conditions: V versus SCE, GCE as working electrode, Bu_4NClO_4 (0.1M) as supporting electrolyte, ODCB/MeCN (4/1) as solvent, 100 mV s^{-1} scan rate. [b] Corresponding to the aldehyde group. [c] In CH_2Cl_2. [d] **27**: 9,10-bis(1,3-dithiol-2-ylidene)-9,10-dihydroanthracene, in

The dyads and triads prepared exhibited an amphoteric redox behavior. Thus, all compounds (**18**, **23**, **25**, **26**) showed the presence of four quasireversible reduction waves, resembling the trend found for the parent C_{60}. These reduction potentials are shifted to more negative values (compared to C_{60}) as a consequence of the partial loss of π conjugation in the C_{60} core. This raises the LUMO energy of the resulting modified fullerene.[19]

On the oxidation side, dyads **18** and **23** show the presence of an electrochemically quasirreversible oxidation wave involving a two-electron process to form the dication, similar to that observed for the parent unsubstituted exTTF **27**.[12] The slightly stronger electron donor ability of **23** can be accounted for by the presence of the electron releasing -O-CH_2- group on the aromatic hydrocarbon skeleton. Triads **25** and **26** exhibit a broad quasirreversible oxidation wave to form the tetracation species. Triad **25**, bearing two identical π-extended TTFs (R″ = H), shows the broad oxidation peak centered at 0.41 V. Similarly, triad **26**, which bears two different π-extended TTFs (R″ = SMe) (see Scheme 2), shows a broad oxidation peak centered at 0.43 V involving the oxidation of both exTTF units. This overlap necessitates determining the oxidation potentials for the respective exTTF units in references **19a** and **19b**.[20]

Photophysical measurements: *C_{60}-extendedTTF dyads*: At first, a series of C_{60}-exTTF dyads (**4a**, **18**, and **23**) were considered to examine the short- and long-range interactions between the two redox-reactive centers at different donor–acceptor separations and compositions (see Figure S2 in the Supporting Information).

Preliminary insight into conceivable implications was taken from steady-state fluorescence experiments. The data were set in relation to a fullerene reference (*N*-methylpyrrolidino[3′,4′:1,2][60]fulllerene, **28**), which lacks the exTTF donor. Owing to the extensive absorption features of exTTFs in the ultraviolet and visible region—which exhibit maxima around 360 and 430 nm—337 nm was chosen as the excitation wavelength to ensure predominant excitation of C_{60}. The absorption ratio between C_{60} and exTTF at 337 nm is approximately 9:1, which still necessitated correction of the fluorescence quantum yields.

Fulleropyrrolidine **28** reveals nearly solvent-independent fluorescence quantum yields (Φ) of 6.0×10^{-4} and fluorescence lifetimes (τ) of 1.5 ns (Table 2). The only observable that changes in room temperature emission measurements is the maximum, which undergoes a moderate red-shift of around 5 nm when moving from toluene towards more polar environments.

In dyads **4a**, **18**, and **23**, a notable quenching of the fullerene fluorescence is seen (Table 2), which, in toluene, reaches a factor of 15 relative to **28**. Upon modifying the solvent polarity from toluene ($\varepsilon = 2.38$) to THF ($\varepsilon = 7.6$) then to dichloromethane ($\varepsilon = 9.08$) and benzonitrile ($\varepsilon = 24.8$) a gradual intensification of the quenching is discernible. An illustration is given in Figure 2 for reference **28** and dyad **18**. We postulate that the underlying solvent dependence is due to an intramolecular electron transfer between the exTTF donor and the photoexcited fullerene (1.76 eV) to yield $C_{60}^{\bullet-}$-$(exTTF)^{\bullet+}$ [Eq. (1)].

Table 2. Fluorescence and singlet excited state features of photoexcited **4a**, **18**, **23**, **25**, **26**, and **28** at room temperature.

	Solvent	τ singlet	τ fluorescence [ns]	Φ fluorescence excited state [ns]
28	toluene	1.35	1.5	6.0×10^{-4}
	THF	1.38	1.5	6.0×10^{-4}
	benzonitrile	1.39	1.41	5.9×10^{-4}
4a	toluene	0.18	0.21	0.4×10^{-4}
	CH_2Cl_2	0.13		0.18×10^{-4}
	benzonitrile	0.08		0.1×10^{-4}
23	toluene	0.57	0.61	3.1×10^{-4}
	THF	0.49	0.50	2.0×10^{-4}
	CH_2Cl_2	0.47	0.45	2.1×10^{-4}
	benzonitrile	0.38	0.36	1.9×10^{-4}
18	toluene	0.45	0.41	2.1×10^{-4}
	THF	0.33	0.29	1.8×10^{-4}
	CH_2Cl_2	0.25	0.21	1.7×10^{-4}
	benzonitrile	0.15		1.1×10^{-4}
25	toluene	0.34	0.36	
	THF	0.21	0.21	
	CH_2Cl_2	0.18	0.18	
	benzonitrile	0.15		
	DMF	0.11		
26	toluene	0.38	0.39	
	THF	0.24	0.25	
	CH_2Cl_2	0.24	0.23	
	benzonitrile	0.18		
	DMF	0.12		

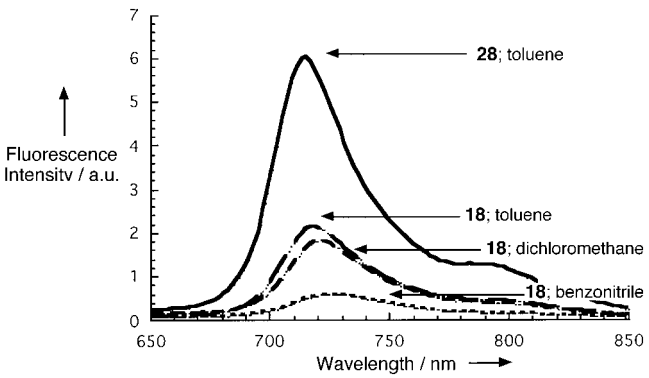

Figure 2. Emission spectra of fulleropyrrolidine **28** in toluene (solid line) and dyad **18** in different solvents (see labels for assignment) with matching absorption at the 337 nm excitation wavelength, $OD_{337\,nm} = 0.5$.

$$C_{60}\text{-}(exTTF) \xrightarrow{h\nu} {}^{1*}C_{60}\text{-}(exTTF) \rightarrow C_{60}^{\bullet-}\text{-}(exTTF)^{\bullet+} \quad (1)$$

The suggestion of a "through-bond" transfer is in sound agreement with the rigid nature of the intervening spacers, which prohibit major conformational rearrangements in the ground and excited state. In fact, theoretical modeling of **4a**, **18**, and **23** (i.e., PM3, see Figure S2 in the Supporting Information) confirms the structural rigidity, ensuring the position of both C_{60} and exTTF in well-defined locations. Extra support for the consideration of an intramolecular electron transfer scenario stems from the thermodynamic driving force determination. This is documented in detail in the Supporting Information.

In dyads **4a**, **18**, and **23** two structural variables are modified to shed light on effects evolving from 1) the donor–acceptor separation and 2) the oxidation strength of the electron donor on the reactivity of photoexcited C_{60}. In line with these alterations, the fullerene fluorescence increases in parallel with larger donor–acceptor separations (i.e., **4a** compared to **23**) and higher oxidation potentials of the donor (i.e., **23** compared to **18**). To illustrate this, the quantum yields in toluene range from around 0.4×10^{-4} (**4a**) to 3.1×10^{-4} (**23**). Similar trends were derived for the quantum yields in more polar THF, dichloromethane, and benzonitrile.

An independent probe for the magnitude of electron transfer quenching is fluorescence lifetime experiments. For this we recorded the 715 nm maximum of the fluorescence in fulleropyrrolidines. Importantly, fluorescence lifetime experiments allow segregating contributions of exTTF from those of C_{60}. In general, the fluorescence decay curves were best fitted by a single exponential decay law. The rate constants ($k = 1/\tau$) agree quite well with those determined indirectly by applying the approximation given in Equation (2).

$$k = 1/\tau_{(\mathbf{4a},\,\mathbf{18},\,\mathbf{23})} = [\Phi_{(\mathbf{28})} - \Phi_{(\mathbf{4a},\,\mathbf{18},\,\mathbf{23})}]/[\tau_{(\mathbf{28})}\Phi_{(\mathbf{4a},\,\mathbf{18},\,\mathbf{23})}] \quad (2)$$

Equation (2) relates the fluorescence quantum yields in the donor–acceptor ensemble $\Phi_{(\mathbf{4a},\,\mathbf{18},\,\mathbf{23})}$ to that of fulleropyrrolidine **28**, $\Phi_{(\mathbf{28})}$, and its lifetime, $\tau_{(\mathbf{28})}$.[21]

To exploit the interactions between photoexcited exTTF and ground-state C_{60}, the former was intentionally excited at 430 nm. The relative absorption ratio between C_{60} and exTTF at 430 nm is 1:9. Although exTTF references emit around 475 nm, which correlates to a singlet excited state energy of ≈2.6 eV, the donor emission remains nearly unaffected in **4a**, **18**, and **23**. Only a marginal quenching of 10% is noted, for example, in toluene. This suggests that exTTFs, once photoexcited, fail to contribute notably to the overall electron and energy transfer reactivity in **4a**, **18**, and **23**. A similar conclusion has been reached for weaker absorbing tetrathiafulvalenes (TTF) in C_{60}-TTF donor-acceptor systems.[22]

In summary, steady-state and time-resolved fluorescence measurements testify that a solvent-dependent and rapid electron transfer decay of the C_{60} singlet excited state prevails in **4a**, **18**, and **23**. To shed light on the nature of the product evolving from this intramolecular deactivation, complementary transient absorption measurements were necessary (i.e., with picosecond to millisecond time-resolution). Following the time evolution of the characteristic singlet excited state features of C_{60}, for instance, is a convenient means of identifying spectral features of the resulting photo-products and to determine absolute rate constants for the intramolecular decay.

Up front, the well-known excited state properties of fulleropyrrolidines (**28**) will be discussed, since they emerge as important reference points for the interpretation of the features expected in dyads **4a**, **18**, and **23**. The singlet excited state, displaying a distinctive singlet–singlet transition around 880 nm, undergoes a quantitative intersystem crossing (ISC) with a rate of 5×10^8 s^{-1}.[23] The ISC process yields the long-lived triplet manifold, for which maxima are noted at 360 and 700 nm, accompanied by a low-energy shoulder at 800 nm.[23]

Detecting the instantaneous appearance (i.e., 18 ps) of the 880 nm absorption affirms the successful C_{60} excitation in dyads **4a**, **18**, and **23** similar to that shown in Figure 3. Instead of seeing, however, the slow ISC dynamics, as **28** exhibits, the singlet–singlet absorption decays in the presence

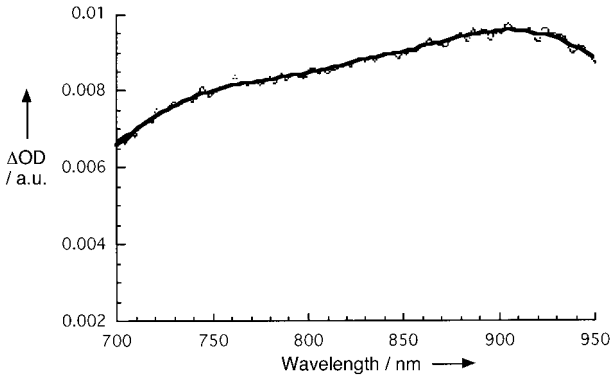

Figure 3. Differential absorption spectra obtained upon picosecond flash photolysis (355 nm) of ≈1.0×10^{-5} M solutions of fulleropyrrolidine **28** in nitrogen-saturated toluene with a time delay of 50 ps.

of exTTF donors with accelerated dynamics. The singlet excited state lifetimes, as determined from an average of first-order fits of the time-absorption profiles at various wavelength (850–950 nm), are listed in Table 2. Spectroscopically, the transient absorption changes, taken after the completion of the decay, bear no resemblance with the C_{60} triplet excited state. In particular, the new transients reveal strong maxima at ≈665 nm, which match those of the one-electron oxidized exTTF radical cations.[24] The spectral differences, namely, of the C_{60} triplet and that of charge-separated radical pair, are illustrated in Figures 4 and 5, respectively.

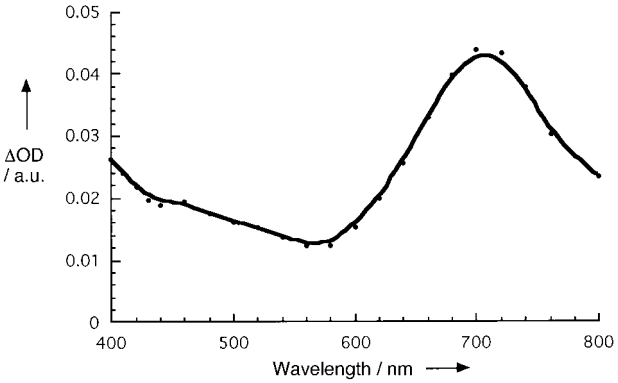

Figure 4. Differential absorption spectra obtained upon nanosecond flash photolysis (337 nm) of ≈1.0×10^{-5} M solutions of fulleropyrrolidine **28** in nitrogen-saturated toluene with a time delay of 50 ns.

An important observation is that the singlet excited state lifetimes match quantitatively those values derived in the fluorescence experiments—steady-state and time-resolved. Overall three trends are established for the fullerene singlet excited state features: The underlying decays decrease as a

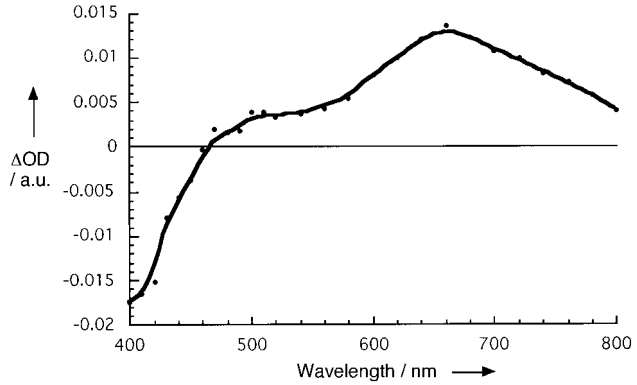

Figure 5. Differential absorption spectra obtained upon nanosecond flash photolysis (337 nm) of $\approx 1.0 \times 10^{-5}$ M solutions of dyad **18** in nitrogen-saturated benzonitrile with a time delay of 50 ns.

function of 1) solvent polarity (**4a**, **18**, and **23**), 2) donor–acceptor separation (**4a** and **23**) and 3) donor strength of the exTTF moiety (**23** and **18**). All these tendencies may be rationalized with respect to the free energy changes associated with an intramolecular electron transfer between the fullerene singlet excited state, the electron acceptor, and the exTTF ground state, the electron donor.

To examine the charge-recombination dynamics, the same dyad solutions were excited with a 6 ns laser pulse. In this context, the spectral fingerprints of the fullerene π-radical anion (1000 nm; $\varepsilon \approx 10000$ $M^{-1}\,cm^{-1}$)[23] and that of the exTTF π-radical cation (665 nm; $\varepsilon \approx 25000$ $M^{-1}\,cm^{-1}$)[24] (Figures 5 and 6, respectively), as seen immediately after the ns laser pulse, are useful probes. It is an important fact that the decay of both probes resemble each other and give rise to kinetics that obey to a clean unimolecular rate law. The rates and quantum yields are listed in Table 3.[25]

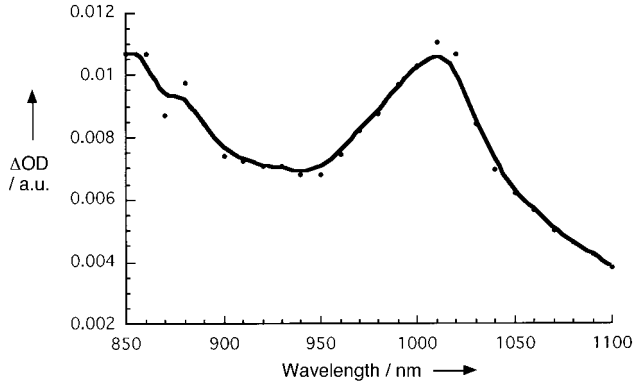

Figure 6. Differential absorption spectra obtained upon nanosecond flash photolysis (337 nm) of $\approx 1.0 \times 10^{-5}$ M solutions of dyad **18** in nitrogen-saturated benzonitrile with a time delay of 50 ns.

A central issue is the stabilization of the charge-separated radical pair as a function of donor–acceptor separations. Strong effects were noted in **4a**. This observation is consistent with our recent report on fullerene derivatives (i.e., [6-5]-open and [6-6]-closed methanofullerenes)[13c] linked directly to a series of exTTF donors. Since upon one-electron oxidation exTTF moieties turn into aromatic and also planar

Table 3. Radical cation characteristics, radical pair lifetimes and radical pair quantum yields in **4a**, **18**, **23**, **25**, and **26** at room temperature.

	Solvent	Radical cation absorption [nm]	Lifetime (τ) radical pair [ns]	Lifetime (τ) radical pair [μs]	Quantum yield (Φ) radical pair	Quantum yield (Φ) radical pair
4a	toluene					
	CH_2Cl_2	660	71		0.39	
	benzonitrile		204		0.1	
23	toluene		54		0.15	
	THF	660	95		0.17	
	CH_2Cl_2		115		0.2	
	benzonitrile		310		0.15	
18	toluene		150		0.13	
	THF	665	310		0.5	
	CH_2Cl_2		322		0.67	
	benzonitrile		460		0.52	
25	toluene		130			
	THF		413	12.1	0.16	0.025
	CH_2Cl_2	665/660				
	benzonitrile		662	54.2	0.28	0.053
	DMF		708	93.1	0.22	0.04
26	toluene		105			
	THF		389	18.9	0.24	0.28
	CH_2Cl_2	680/660				
	benzonitrile		582	85.1	0.28	0.14
	DMF		664	111	0.22	0.11

scaffolds, thus rendering the reverse reduction process to the neutral molecule more difficult, both parameters provide additional stabilization forces for the radical pair.

Extending the donor-acceptor separation from 9.5 Å (**4a**) to 14.0 Å (**23**), while keeping the thermodynamics unchanged, led to a surprising observation. Instead of the expected large increase in radical pair lifetime, as observed in C_{60}–porphyrin systems, only a moderate (66%) improvement was seen.[26] This leads us to assume that the stabilization forces, as they stem from the gain of aromaticity/planarity, impose much stronger bearings on the radical pair at shorter separations as in dyad **4a**. At larger separations, for example in dyad **23**, the electronic coupling (V) becomes the dominant factor controlling the kinetics.

C_{60}-extendedTTF-extendedTTF triads[27]: We note the following structural features: Dyad **18** and triads **25** and **26** bear the same C_{60}-exTTF primary building block. In this context, it is vital to realize that the composition of this subunit controls the deactivation of the fullerene singlet excited state, while the presence of a second exTTF donor or fullerene acceptor is, to a large degree, irrelevant to the initial charge-separation event. The fluorescence lifetimes of **25** are practically identical to those listed for dyad **18** (Table 2). This supports the notion that the photoexcited fullerene in **18**, and **25** indeed deactivates in a similar manner.

Regarding the picosecond transient absorption measurements, immediately, after the 18 ps laser excitation of **25**, the strong singlet-singlet absorption of the fullerene (λ_{max} at 900 nm) was found (Figure 7).[21] Despite the presence of two exTTFs, this once again confirms the successful formation of the fullerene singlet excited state. Similar to **4a**, **18**, and **23**

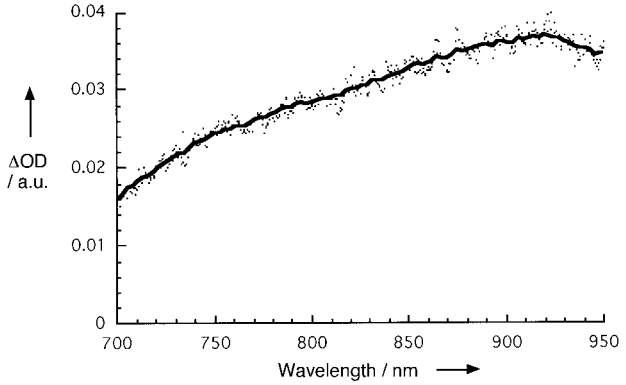

Figure 7. Differential absorption spectra obtained upon picosecond flash photolysis (355 nm) of $\approx 1.0 \times 10^{-5}$ M solutions of triad **25** in nitrogen-saturated benzonitrile with a time delay of 50 ps.

(see above) the fullerene singlet excited state is subject to a solvent-dependent decay. Also in the case of **25**, the product of the initial decay is the charge-separated radical pair, that is, $C_{60}^{\bullet-}$ and $(exTTF)^{\bullet+}$.[28] In light of the two exTTF electron donors, which support an additional intramolecular charge-shift reaction ($-\Delta G_{CS} = 0.06$ eV), that is, $(exTTF)_1^{\bullet+} \rightarrow (exTTF)_2^{\bullet+}$, we analyzed the picosecond kinetics in depth [Eq. (3)]. All attempts to monitor this charge-shift failed, indicating that this intramolecular reaction constitutes either only a minor component and/or takes place with dynamics that are out of our assessable time domain (i.e., 18 – 5000 ps).

$$C_{60}\text{-}(exTTF)_1\text{-}(exTTF)_2 \xrightarrow{h\nu} {}^1{*}C_{60}\text{-}(exTTF)_1\text{-}(exTTF)_2 \rightarrow C_{60}^{\bullet-}\text{-}(exTTF)_1^{\bullet+}\text{-}(exTTF)_2 \quad (3)$$

The transient absorption changes, recorded 50 ns after 6 ns laser excitation, reveal the attributes for the one-electron oxidized exTTF ($\lambda_{max} \approx 665$ nm) and that of the one-electron reduced fullerene ($\lambda_{max} \approx 1000$ nm)—compare Figure 5 and 6. The decay dynamics of the radical pair absorption, as typically recorded on the nanosecond/microsecond timescale, gives rise to a two-component decay (Figure 8, DMF). The faster segment reveals a lifetime of several hundred nanoseconds, while the slower segment lies in the range of several tens of microseconds, see Table 3. Both decay components were best fitted by first-order kinetics, confirming intramolecular reactions.[29]

Interestingly, not only are the decay rates of the short-lived species identical with those of dyad **18**, but also their spectral features (i.e., $\lambda_{max} \approx 665$ nm) are superimposable. From these kinetic and spectroscopic arguments we must infer that the origin of this product is the adjacent radical pair, $C_{60}^{\bullet-}$-$(exTTF)_1^{\bullet+}$-$(exTTF)_2$.

By analyzing the exTTF radical cation absorption we noted some differences between the maximum of the short-lived and long-lived species of about 5 nm (i.e., 665 → 660 nm). This can be reasonably correlated with the changes in the chemical substitution of the two disparate exTTF donors, namely, $(exTTF)_1$ and $(exTTF)_2$. Consequently, we postulate that the long-lived product is the distant radical pair, namely, $C_{60}^{\bullet-}$-$(exTTF)_1$-$(exTTF)_2^{\bullet+}$ [Eq. (4)].

$$C_{60}^{\bullet-}\text{-}(exTTF)_1^{\bullet+}\text{-}(exTTF)_2 \rightarrow C_{60}^{\bullet-}\text{-}(exTTF)_1\text{-}(exTTF)_2^{\bullet+} \quad (4)$$

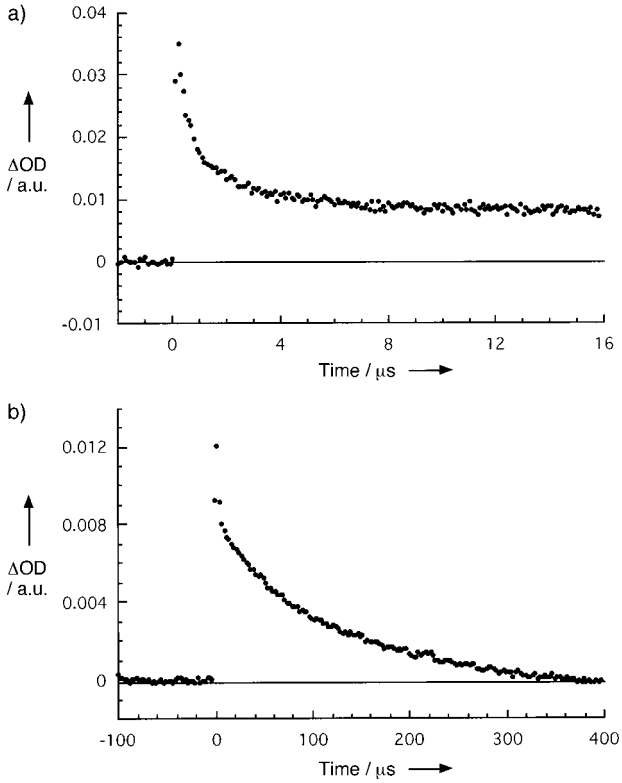

Figure 8. Time-absorption profiles at 1000 nm monitoring the fullerene radical anion decay dynamics of a) $C_{60}^{\bullet-}$-$(exTTF)_1^{\bullet+}$-$(exTTF)_2$ and b) $C_{60}^{\bullet-}$-$(exTTF)_1$-$(exTTF)_2^{\bullet+}$ in triad **25** in nitrogen-saturated DMF.

In a detailed pulse radiolytic work,[24] we demonstrated that λ_{max} is impacted by the substitution pattern of the exTTF derivative. In fact, the maximum for the parent exTTF π-radical cation is found at 660 nm, which resembles that of the distant radical pair.

Determining the quantum yields of charge-separation (see Table 3) for the two radical pairs, namely, $C_{60}^{\bullet-}$-$(exTTF)_1^{\bullet+}$-$(exTTF)_2$ and $C_{60}^{\bullet-}$-$(exTTF)_1$-$(exTTF)_2^{\bullet+}$ led to the conclusion that the distant and long-lived radical pair is being formed in minor yields. The thermodynamics estimated for **25** unveil that a charge-shift reaction between the two adjacent exTTF moieties (i.e., $(exTTF)_1^{\bullet+} \rightarrow (exTTF)_2^{\bullet+}$) has a small driving force, -0.06 eV. Consequently, the formation of the distant radical pair can only be rationalized in terms of an existing equilibrium. Applying the energy difference between the two states, we estimate quantum yields of ≈15 % relative to that of the adjacent radical pair, which is in satisfying agreement with the experimental values.[30]

Raising the oxidation potential of the exTTF moiety neighboring the fullerene leads to a number of important consequences. First, it clearly decreases the driving force for the initial electron transfer starting from the photoexcited fullerene in triad **26**. Second, it effects the charge-shift reaction towards the distant radical pair ($-\Delta G_{CS} = 0.17$ eV). The first outcome should have no implications, since the free energy changes associated with the initial intramolecular electron transfer are sufficiently exothermic that increasing the oxidation potential (i.e., comparing **25** with **26**) still guarantees activation of the electron transfer process. By

contrast, altering the charge-shift driving forces is expected to have a more subtle impact, namely, to facilitate mediation of the positive charge to the remote end of the linear triad, the distant $C_{60}^{\bullet-}$-$(exTTF)_1$-$(exTTF)_2^{\bullet+}$ radical pair.

As far as the emission studies are concerned, the fullerene fluorescence lifetime is surely lengthened in **26** relative to **25**. This reflects the smaller free energy changes ($-\Delta G_{CS}$) in **26**. From the transient absorption measurements, a parallel trend was measured for the singlet excited state lifetimes. In general, the deactivation rates differ between these two C_{60}-exTTF-exTTF triads by around 20%.

The differential absorption changes, recorded at the end of the charge-separation process (200–400 ps), disclosed dissimilar transient species in the two different triads (**25** and **26**). While we registered a λ_{max} at 665 nm for **25**, **26** has its strongest absorption at 680 nm (Figure 9a). As stated above, our independent pulse-radiolysis work[24] led to a maximum for a S–Me derivative (resembling that in **26**) at 675 nm. Based

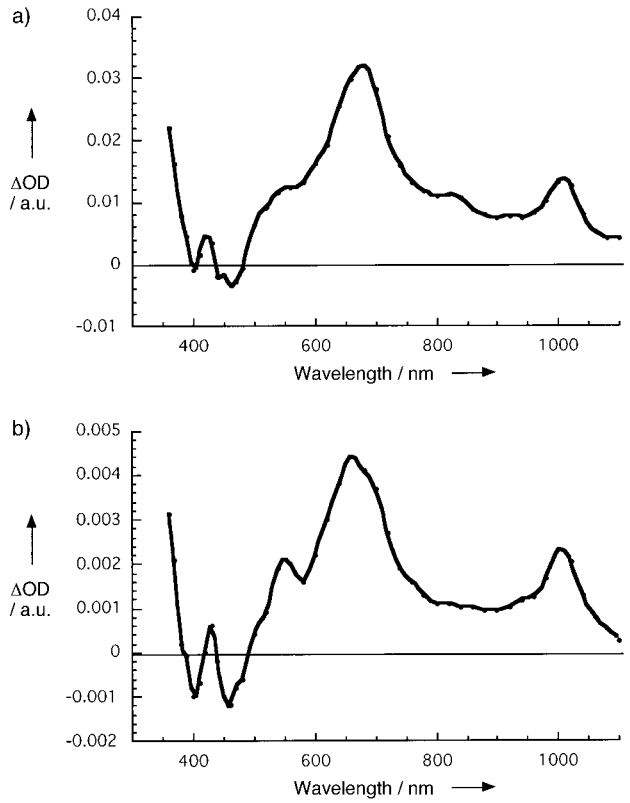

Figure 9. Differential absorption spectra obtained upon nanosecond flash photolysis (337 nm) of $\approx 1.0 \times 10^{-5}$ M solutions of triad **26** in nitrogen-saturated benzonitrile with a time delay of a) 50 ns, $C_{60}^{\bullet-}$-$(exTTF)_1^{\bullet+}$-$(exTTF)_2$ and b) 2000 ns $C_{60}^{\bullet-}$-$(exTTF)_1$-$(exTTF)_2^{\bullet+}$.

on this spectral similarity, we conclude the successful generation of the adjacent radical pair.[31]

Again, two major decays were noted in triad **26**, which support the presence of both radical pairs, namely, adjacent (λ_{max} at 680 nm, Figure 9a) and distant (λ_{max} at 660 nm, Figure 9b). These represent a fast step occurring on a timescale of several hundred nanoseconds and a slower one, which yields lifetimes that typically vary between 18.9 and 111 μs in THF and DMF, respectively. Inspection of the energy gap dependence, as varied by the solvent dependence, leads to the conclusion that both charge-recombination processes are also in the normal region of the Marcus-parabola (i.e., $-\Delta G_{CR} < \lambda$). Due to the smaller energy gap ($-\Delta G_{CR}$) in **25**, charge-recombination within the adjacent pair is slowed-down by about 10% relative to that **26**.

In line with the concept of modulating the redox gradient to control the distant radical pair, the quantum yield of the latter increased up to 50%. Interestingly, although the energies of the $C_{60}^{\bullet-}$-$(exTTF)_1$-$(exTTF)_2^{\bullet+}$ radical pair in **25** and **26** are identical, notable changes are seen in the corresponding lifetimes. In particular, lowering the energy of the distant radical pair below that of the adjacent one slows-down the charge-recombination. In DMF, 93.1 μs should be compared to 111 μs for **25** and **26**, respectively.

Considering donor–acceptor separations of about 30 Å, electronic coupling within the distant radical pair is weak and will not change notably between triad **25** and **26**.[32] A temperature dependence of the intramolecular charge recombination rates gave further insight into the thermally activated barrier. The Arrhenius plot (Figure 10) for triad **26** in deoxygenated

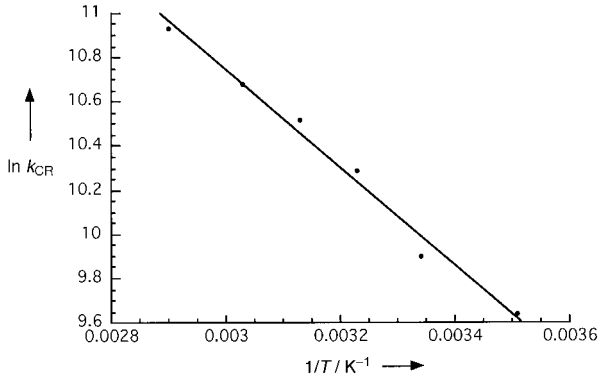

Figure 10. Arrhenius plot of intramolecular charge recombination in triad **26** in deoxygenated benzonitrile.

benzonitrile gives rise to a good linear relationship between ln k_{CR} and 1/T. The activation barrier (E_a), as determined from the slope, is 0.16 eV, which agrees with the difference in energy level between $C_{60}^{\bullet-}$-$(exTTF)_1$-$(exTTF)_2^{\bullet+}$ and $C_{60}^{\bullet-}$-$(exTTF)_1^{\bullet+}$-$(exTTF)_2$. Given the good agreement between activation barrier (E_a) and energy gap ($-\Delta G_{CS}$), we conclude that $C_{60}^{\bullet-}$-$(exTTF)_1$-$(exTTF)_2^{\bullet+}$ deactivates by means of a stepwise electron transfer mechanism (see Equation (5)) rather than a concerted mechanism (see Equation (6).)[33]

$$C_{60}^{\bullet-}\text{-}(exTTF)_1\text{-}(exTTF)_2^{\bullet+} \rightarrow C_{60}^{\bullet-}\text{-}(exTTF)_1^{\bullet+}\text{-}(exTTF)_2 \rightarrow C_{60}\text{-}(exTTF)_1\text{-}(exTTF)_2 \quad (5)$$

$$C_{60}^{\bullet-}\text{-}(exTTF)_1\text{-}(exTTF)_2^{\bullet+} \rightarrow C_{60}\text{-}(exTTF)_1\text{-}(exTTF)_2 \quad (6)$$

Conclusions

We have described the multistep synthesis of novel electroactive dyads (**18** and **23**) and triads (**25** and **26**) by 1,3-dipolar cycloaddition reactions of azomethine ylides generated in situ, endowed with the strong electron donor exTTFs, to C_{60}.

In order to carry out a systematic study, different rigid chemical spacers and substitution patterns on the donor moiety have been used for the dyads, while the same chemical spacer was used to evaluate the effect that a second donor unit has on the electrochemical and photophysical properties in these rigid ensembles. It is worth mentioning that the synthesis of the reported compounds is rather complex and, thus, compound **26** requires twenty synthetic steps for its preparation.

Donor–acceptor distances between 9.5 and 15.3 Å prevent substantial charge transfer character in the ground state, as, for example, confirmed in cyclic voltammetry and absorption spectroscopy. Only upon photoexcitation of the fullerene chromophore rapid and efficient charge transfer is seen, which yields $C_{60}^{\bullet-}$-(exTTF)$^{\bullet+}$ (**4a**, **18**, **23**) and $C_{60}^{\bullet-}$-(exTTF)$^{\bullet+}$-(exTTF) (**25**, **26**). For dyads **4a**, **18**, and **23** charge recombination follows directly and regenerates quantitatively the singlet ground state. In the triads, on the other hand, sequential electron transfer by means of the transient adjacent radical pair [$C_{60}^{\bullet-}$-(exTTF)$^{\bullet+}$-(exTTF)] transforms the fullerene singlet excited state ultimately into the distant radical pair [$C_{60}^{\bullet-}$-(exTTF)-(exTTF)$^{\bullet+}$], for which we determined lifetimes of up to 111 μs in DMF. These values have never previously been accomplished in molecular triads. Notable couplings and small energy gaps between the adjacent and distant radical pair in dyads **25** and **26** lead to a stepwise charge recombination mechanism (Scheme 3).

Experimental Section

Synthesis of fulleropyrrolidine dyads and triads: general procedure: A solution of C_{60} (0.138 mmol), the corresponding aldehyde (0.166 mmol for **17** and 0.064 mmol for **22**, **24a** and **24b**) and *N*-methylglycine (0.5 mmol) in toluene (100 mL) was refluxed for 16 h. Then the solvent was removed under reduced pressure and the crude material was carefully chromatographed on a silica gel column using chloroform as eluent. Further purification was accomplished by repetitive precipitation and centrifugation by using methanol as solvent.

Dyad C_{60}-exTTF (18): 61% yield; m.p. > 300 °C (decomp); ^{1}H NMR (300 MHz, $CDCl_3$:CS_2, 25 °C): δ = 8.30 (d, ^3J(H,H) = 8.7 Hz, 2H), 8.01 (br s, 2H), 7.66 (d, ^3J(H,H) = 8.4 Hz, 1H), 7.52 (d, ^3J(H,H) = 8.4 Hz, 1H), 7.48 (d, ^4J(H,H) = 2.4 Hz, 1H), 7.15 (d, ^4J(H,H) = 2.4 Hz, 1H), 7.10 (dd, $^3J_1$(H,H) = 8.4 Hz, $^4J_2$(H,H) = 2.4 Hz, 1H), 6.76 (dd, $^3J_1$(H,H) = 8.4 Hz, $^4J_2$(H,H) = 2.4 Hz, 1H), 6.30 (d, ^3J(H,H) = 12 Hz, 4H), 5.10 (s, 1H), 5.07 (d, ^3J(H,H) = 9.6 Hz, 1H), 4.37 (d, ^3J(H,H) = 9.6 Hz, 1H), 4.01 (t, ^3J(H,H) = 7.5, 2H), 2.89 (s, 3H), 1.83 (q, ^3J(H,H) = 7.7 Hz, 2H), 1.51–1.39 (m, 6H), 0.91 ppm (m, 3H); ^{13}C NMR (125 MHz, $CDCl_3$:CS_2, 25 °C): δ = 164.4, 157.2, 152.7, 152.3, 147.3, 146.3, 145.9, 145.7, 145.6, 145.2, 144.7, 144.3, 143.1, 143.0, 142.6, 142.1, 141.7, 140.2, 137.0, 136.0, 135.6, 133.1, 130.6, 130.0, 129.5, 128.1, 126.0, 125.8, 118.5, 118.2, 117.3, 112.2, 110.9, 83.1, 69.9, 69.0, 68.2, 61.0, 40.0, 31.8, 29.9, 25.9, 22.8, 14.2 ppm; FTIR (KBr) 125 MHz: $\tilde{\nu}$ = 2921, 2850, 2777, 1733, 1600, 1543, 1506, 1460, 1410, 1243, 1196, 1101, 1062, 1016, 635, 525 cm^{-1}; UV/Vis (CH_2Cl_2): λ_{max} (log ε) = 254 (4.84), 276 (4.77), 310 (4.56), 432 (4.30) nm; MS (MALDI-TOF): *m*/*z* (%) 1376 (100) [M^+].

Dyad C_{60}-exTTF (23): 61% yield; m.p. > 300 °C (decomp); ^{1}H NMR (300 MHz, $CDCl_3$, 25 °C): δ = 8.16 (d, ^3J(H,H) = 8.4 Hz, 2H), 8.10 (d, ^3J(H,H) = 8.0 Hz, 1H), 7.90 (br s, 2H), 7.76 (d, ^4J(H,H) = 1.8 Hz, 1H), 7.65 (m, 2H), 7.34 (dd, $^3J_1$(H,H) = 8.0 Hz, $^4J_1$(H,H) = 1.8 Hz, 1H), 7.28 (m, 2H), 6.28 (m, 4H), 5.43 (s, 2H), 5.02 (d, ^3J(H,H) = 9.5 Hz, 1H), 5.01 (s, 1H), 4.30 (d, ^3J(H,H) = 9.5 Hz 1H), 2.82 ppm (s, 3H); ^{13}C NMR (75 MHz, $CDCl_3$:CS_2, 25 °C): δ = 165.9, 156.7, 153.8, 152.6, 152.3, 146.4, 146.3, 146.2, 146.1, 146.0, 145.8, 145.7, 145.6, 145.5, 145.4, 145.3, 145.2, 145.1, 145.0, 144.6, 144.5, 144.3, 144.2, 143.0, 142.9, 142.6, 142.5, 142.4, 142.3, 142.2, 142.1, 142.0, 141.9, 141.8, 141.6, 141.4, 140.1, 139.8, 139.5, 136.8, 136.3, 135.8, 135.6, 135.5, 135.2, 135.1, 135.0, 133.4, 130.2, 130.1, 129.9, 129.2, 128.9, 128.1, 125.9, 125.7, 125.2, 125.1, 124.9, 124.8, 124.6, 121.7, 117.2, 117.1, 117.0, 83.0, 76.8, 69.9, 67.6, 66.7, 39.9 ppm; FTIR (KBr): $\tilde{\nu}$ = 1744, 1541, 1507, 1451, 1424, 1384, 1365, 1284, 1265, 1231, 1186, 1033, 762, 744, 576, 526 cm^{-1}; UV/Vis (CH_2Cl_2): λ_{max} (log ε) = 254 (4.84), 276 (4.77), 310 (4.56), 432 (4.30) nm; MS (MALDI-TOF): *m*/*z* (%) 1290 (100) [M^+].

Triad C_{60}-exTTF$_1$-exTTF$_1$ (25): 43% yield, m.p. > 300 °C (decomp); ^{1}H NMR (300 MHz, $CDCl_3$:CS_2, 25 °C): δ = 8.30 (d, ^3J(H,H) = 9 Hz, 2H), 8.20 (d, ^3J(H,H) = 9 Hz, 2H), 8.05 (br s, 2H), 7.85 (s, 1H), 7.78–7.58 (m, 8H), 7.48 (dd, $^3J_1$(H,H) = 6 Hz, $^4J_1$(H,H) = 1.2 Hz, 1H), 7.32–7.24 (m, 5H), 7.17 (m, 2H), 6.34 (m, 8H), 5.10 (s, 1H), 5.07 (d, ^3J(H,H) = 8.2 Hz, 1H) 4.36 (d, ^3J(H,H) = 8.2 Hz, 1H), 2.89 ppm (s, 3H); ^{13}C NMR (125 MHz, $CDCl_3$:CS_2, 25 °C): δ = 164.0, 155.6, 153.4, 152.6, 152.2, 148.4, 147.1, 146.1, 145.9, 145.7, 145.4, 145.1, 144.5, 144.2, 142.9, 142.7, 142.5, 142.4, 141.9, 141.8, 141.5, 140.0, 139.8, 139.4, 137.3, 136.8, 136.6, 136.3, 135.8, 135.4, 135.0, 134.1, 132.9, 131.9, 130.5, 130.1, 129.6, 129.3, 128.0, 127.2, 126.3, 125.9, 125.6, 125.2, 124.8, 124.5, 123.1, 121.8, 120.4, 118.6, 118.0, 117.1, 82.9, 69.8, 68.8, 39.8 ppm; FTIR (KBr): $\tilde{\nu}$ = 2927, 1733, 1718, 1701, 1683, 1652, 1602, 1558, 1541, 1508, 1488, 1257, 1176, 1112, 1068, 1014, 800, 704, 526 cm^{-1}; UV/Vis (CH_2Cl_2): λ_{max} (log ε) = 252 (4.74), 278 (4.72), 330 (4.51), 431 (4.23) nm; MS (MALDI-TOF): *m*/*z* (%): 1801 (100) [M^+].

Triad C_{60}-exTTF$_1$-exTTF$_2$ (26): 51% yield, m.p. > 300 °C (decomp); ^{1}H NMR (300 MHz, $CDCl_3$:CS_2, 25 °C): δ = 8.32 (d, ^3J(H,H) = 9.5 Hz, 2H), 8.23 (d, ^3J(H,H) = 8.4 Hz, 2H), 7.92 (br s, 2H), 7.78–7.66 (m, 6H), 7.60 (d, ^3J(H,H) = 8.4 Hz), 7.57–7.43 (m, 2H), 7.32 (m, 2H), 6.35 (m, 4H), 5.07 (s, 1H), 5.04 (d, ^3J(H,H) = 8.8 Hz, 1H) 4.33 (d, ^3J(H,H) = 8.8 Hz, 1H), 2.85 (s, 3H), 2.42 ppm (s, 12H); ^{13}C NMR (125 MHz, $CDCl_3$:CS_2, 25 °C): δ = 164.0, 155.8, 153.1, 152.7, 152.5, 148.2, 147.0, 146.4, 145.8, 145.6, 145.4, 144.6,

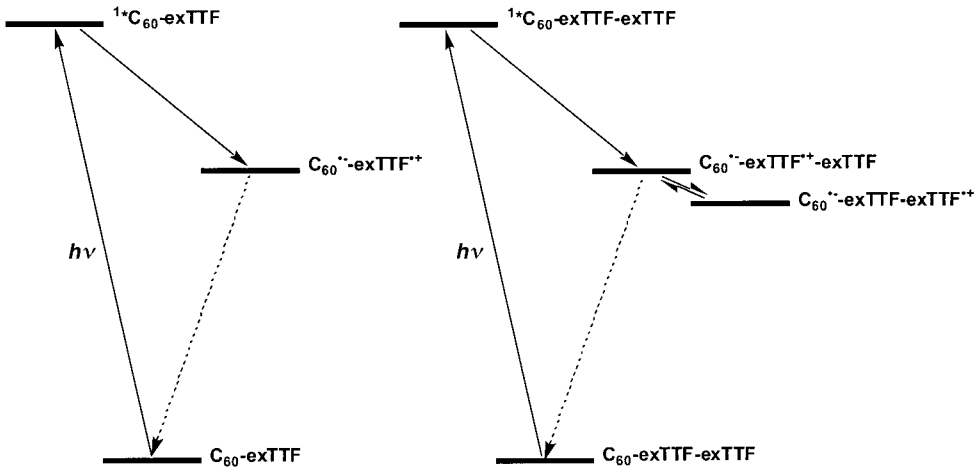

Scheme 3. Possible charge-recombination mechanisms for the systems discussed.

144.4, 144.3, 143.3, 143.1, 142.7, 142.6, 142.5, 142.2, 142.2, 142.1, 142.0, 141.9, 141.7, 141.6, 140.2, 139.9, 136.2, 136.1, 136.0, 135.9, 135.6, 135.5, 135.2, 132.5, 132.3, 132.2, 131.5, 130.8, 130.7, 130.6, 130.5, 129.6, 129.5, 128.8, 126.5, 126.3, 126.0, 125.9, 125.4, 124.9, 124.7, 124.4, 123.2, 122.0, 121.9, 119.4, 119.3, 118.6, 118.3, 117.3, 82.8, 69.8, 68.8, 39.9, 19.1 ppm; FTIR (KBr): $\tilde{\nu}$ = 2927, 1733, 1718, 1701, 1683, 1652, 1602, 1558, 1541, 1508, 1488, 1257, 1176, 1112, 1068, 1014, 800, 704, 526 cm^{-1}; UV/Vis (CH_2Cl_2): λ_{max} (log ε) = 252 (4.74), 278 (4.72), 330 (4.51), 431 (4.23) nm; MS (MALDI-TOF): *m*/*z* (%): 1985 (100) [M^+].

Acknowledgements

We are indebted to MCYT of Spain (Project BQU2002–00855) and the Office of Basic Energy Sciences of the U.S. Department of Energy (contribution No. NDRL-4444 from the Notre Dame Radiation Laboratory) for financial support.

[1] a) J. Deisenhofer, O. Epp, K. Miki, R. Huber, H. Michel, *J. Mol. Biol.* **1984**, *180*, 385; b) W. Rettig, *Angew. Chem.* **1986**, *98,* 969–986; *Angew. Chem. Int. Ed. Engl.* **1986**, *25*, 971–988; c) T. J. Meyer, *Acc. Chem. Res.* **1989**, *22*, 163–170.

[2] a) J. S. Connolly, J. R. Bolton in *Photoinduced Electron Transfer* (Eds.: M. A. Fox, M. Chanon), Elsevier, Amsterdam, **1988**, Part D, pp. 303–393; b) M. R. Wasielewski in *Photoinduced Electron Transfer* (Eds.: M. A. Fox, M. Chanon), Elsevier, Amsterdam, **1988**, Part A, pp. 161–206.

[3] a) M. R. Wasielewski, *Chem. Rev.* **1992**, *92*, 435–461; b) M. Bixon, J. Fajer, G. Feher, J. H. Freed, D. Gamliel, A. J. Hoff, H. Levanon, D. Möbius, J. R. Norris, R. Nechushtai, A. Scherz, J. L. Sessler, D. H. A. Stehlik, *Isr. J. Chem.* **1992**, *32*, 369; c) D. Gust, T. A. Moore, A. L. Moore, *Acc. Chem. Res.* **1993**, *26*, 198–205; d) H. Kurreck, M. Huber, *Angew. Chem.* **1995**, *107*, 929–947; *Angew. Chem. Int. Ed. Engl.* **1995**, *34*, 849—866; e) D. Gust, T. A. Moore in *The Porphyrin Handbook*, *Vol. 8* (Eds.: K. M. Kadish, R. Smith, R. Guilard), Academic Press, San Diego, CA, **2000**, pp. 153–190; f) D. Gust, T. A. Moore, A. L. Moore, *Acc. Chem. Res.* **2001**, *34*, 40–48; g) D. M. Guldi, N. Martín, *J. Mat. Chem.* **2002**, *12*, 1978–1992.

[4] a) J.-C. Chambron, S. Chardon-Noblat, A. Harriman, V. Heitz, J. P. Sauvage, *Pure Appl. Chem.* **1993**, *65*, 2343; b) A. Harriman, J.-P. Sauvage, *Chem. Soc. Rev.* **1996**, *26*, 41–48; c) M.-J. Blanco, M. C. Jiménez, J.-C. Chambron, V. Heitz, M. Linke, J.-P. Sauvage, *Chem. Soc. Rev.* **1999**, *28*, 293–306; d) V. Balzani, A. Juris, M. Venturi, S. Campagna, S. Serroni, *Chem. Rev.* **1996**, *96*, 759–834; e) *Electron Transfer in Chemistry* (Ed.: V. Balzani), Wiley-VCH, Weinheim, **2001**.

[5] a) M. N. Paddon-Row, *Acc. Chem. Res.* **1994**, *27*, 18–25; b) J. W. Verhoeven in *Electron Transfer—From Isolated Molecules to Biomolecules*, *Part 1*, (Eds.: J. Jortner, M. Bixon), Wiley, New York, **1999**, pp. 603–644; c) K. Maruyama, A. Osuka, *Pure Appl. Chem.* **1990**, *62*, 1511; d) K. Maruyama, A. Osuka, N. Mataga, *Pure Appl. Chem.* **1994**, *66*, 867; e) A. Osuka, N. Mataga, T. Okada, *Pure Appl. Chem.* **1997**, *69*, 796–802; f) L. Sun, L. Hammarström, B. Åkermark, S. Styring, *Chem. Soc. Rev.* **2001**, *30*, 36–49.

[6] a) D. M. Guldi, K.-D. Asmus, *J. Am. Chem. Soc.* **1997**, *119*, 5744–5745; b) H. Imahori, K. Hagiwara, T. Akiyama, M. Aoki, S. Taniguchi, T. Okada, M. Shirakawa, Y. Sakata, *Chem. Phys. Lett.* **1996**, *263*, 545–550; c) D. M. Guldi, *Chem. Soc. Rev.* **2002**, *31*, 22–36.

[7] a) *Fullerenes: From Synthesis to Optoelectronic Properties* (Eds.: D. M. Guldi, N. Martín), Kluwer, Dordrecht, **2002**; b) *Fullerenes and Related Structures, Vol. 199* (Ed.: A. Hirsch), Springer, Berlin, **1999**.

[8] a) N. Martín, L. Sánchez, B. Illescas, I. Pérez, I. *Chem. Rev.* **1998**, *98*, 2527–2548; b) H. Imahori, Y. Sakata, *Adv. Mater.* **1997**, *9*, 537–546; c) H. Imahori, Y. Sakata, *Eur. J. Org. Chem.* **1999**, *64*, 2445–2457.

[9] a) P. Barbara, T. J. Meyer, M. A. Ratner, *J. Phys. Chem.* **1996**, *100*, 13148–13168; b) P. Piotrowiak, *Chem. Soc. Rev.* **1999**, *28*, 143–150; c) C. C. Moser, J. M. Keske, K. Warncke, R. S. Farid, P. L. Dutton, *Nature* **1992**, *355*, 796–802.

[10] a) N. Martín, L. Sánchez, M. A. Herranz, D. M. Guldi, *J. Phys. Chem. A.* **2000**, *104*, 4648–4657; b) D. M. Guldi, S. González, N. Martín, A. Antón, J. Garín, J. Orduna, *J. Org. Chem.* **2000**, *65*, 1978–1983.

[11] For a recent review on TTF, see: J. L. Segura, N. Martín, *Angew. Chem.* **2001**, 113, 1416–1455; *Angew. Chem. Int. Ed.* **2001**, *40*, 1372–1409.

[12] a) N. Martín, L. Sánchez, C. Seoane, E. Ortí, P. M. Viruela, R. Viruela, *J. Org. Chem.* **1998**, *63*, 1268–1279; b) M. R. Bryce, A. J. Moore, M. Hasan, G. J. Ashwell, A. T. Fraser, W. Clegg, A. I. Hursthouse, M. B. Karaulov, *Angew. Chem.* **1990**, 102, 1493–1495; *Angew. Chem. Int. Ed. Engl.* **1990**, *29*, 1450–1452; c) Y. Yamashita, Y. Kobayashi, T. Miyashi, *Angew. Chem.* **1989**, 101, 1090–1091; *Angew. Chem. Int. Ed. Engl.* **1989**, *28*, 1052–1053; d) N. Martín, I. Pérez, L. Sánchez, C. Seoane, *J. Org. Chem.* **1997**, *62*, 870–877.

[13] a) N. Martín, I. Pérez, L. Sánchez, C. Seoane, *J. Org. Chem.* **1997**, *62*, 5690–5695; b) M. A. Herranz, N. Martín, *Org. Lett.* **1999**, *1*, 2005–2007; c) N. Martín, L. Sánchez, D. M. Guldi, *Chem. Commun.* **2000**, 113–114.

[14] a) M. Maggini, G. Scorrano, M. Prato, *J. Am. Chem. Soc.* **1993**, *115*, 9798–9799; b) M. Prato, M. Maggini, *Acc. Chem. Res.* **1998**, *31*, 519–526.

[15] G. J. Marshallay, M. R. Bryce, *J. Org. Chem.* **1994**, *59*, 6847–6849.

[16] R. Gómez, PhD thesis, Universidad Complutense de Madrid (Spain), **2001**.

[17] a) Compound **20** was obtained in a three-step procedure from commercially available 2-hydroxymethyl-anthraquinone. See: S. González, N. Martín, D. M. Guldi, *J. Org. Chem.* **2003**, *68*, 779–791; b) I. Pérez, PhD thesis, Universidad Complutense de Madrid (Spain), **2003**.

[18] a) B. Illescas, M. A. Martínez-Grau, M. L. Torres, J. Fernández-Gadea, N. Martín, *Tetrahedron Lett.* **2002**, *43*, 4133–4136; b) T. Gu, C. Bourgogne, J. F. Nierengarten, *Tetrahedron Lett.* **2001**, *42*, 7249–7252; c) P. de la Cruz, A. de la Hoz, L. A. Font, F. Langa, M. C. Pérez-Rodriguez, *Tetrahedron Lett.* **1998**, *39*, 6053–6056.

[19] a) T. Suzuki, Y. Maruyama, T. Akasaba, W. Ando, K. Kobayashi, S. Nagase, *J. Am. Chem. Soc.* **1994**, *116*, 1359–1363; b) L. Echegoyen, L. E. Echegoyen, *Acc. Chem. Res.* **1998**, *31*, 593–601.

[20] The aforementioned redox potentials indicate the absence of significant electronic interaction between the electroactive chromophores in **18**, **23**, **25**, and **26**.

[21] We would like to point out that the missing data points in Table 2 could not be determined within the 100 ps time-resolution of the apparatus. The complementary picosecond-resolved transient absorption measurements infer indeed lifetimes that are either close to or within the 100 ps apparatus time-resolution.

[22] G. Kodis, P. A. Liddell, L. de la Garza, A. L. Moore, T. A. Moore, D. Gust, *J. Mater. Chem.* **2002**, 2100–2108.

[23] D. M. Guldi, M. Prato, *Acc. Chem. Res.* **2000**, *33*, 695–703.

[24] D. M. Guldi, L. Sánchez, N. Martín, *J. Phys. Chem. B* **2001**, *105*, 7139–7144.

[25] The charge-recombination rates are smaller in polar than in nonpolar solvents. This relationship suggests that the rate constants are in the normal region of the Marcus parabola ($-\Delta G_{CR} < \lambda$). Considering the structural changes that the one-electron oxidation of exTTFs causes, the reorganization energy of the radical pair is assumed to be quite large. In addition, the $-\Delta G_{CR}$ values are insufficiently large as to surpass the reorganization energy in **4a**, **18**, and **23** ($-\Delta G_{CR} \approx \lambda$), which would shift the charge-recombination into the inverted region of the Marcus parabola ($-\Delta G_{CR} > \lambda$).

[26] Interestingly, the lifetime of **23**, which is in the range of several hundred nanoseconds, is virtually comparable to those found in C_{60}–donor dyads with a similar spacer (see reference [6c]).

[27] The reactivity scheme of **4a**, **18**, and **23**—comparing the steady-state and time-resolved fluorescence experiments—fails to reveal substantial differences. Therefore, only time-resolved fluorescence lifetime measurements will be discussed for triads **25** and **26**. In addition, the presence of two exTTF moieties imposes notable difficulties on convoluting the individual contributions in the steady-state emission experiments.

[28] The intramolecular decay rates in triad **26** do not differ notably from those of dyad **18**.

[29] Additional proof for an intramolecular charge-recombination stems from a set of experiments, conducted with different laser power and different dyad concentrations: Decreasing the radical-pair concen-

tration in various increments by up to 65% failed to lead to any notable changes in the charge-recombination kinetics.

[30] Determined by means of $\Delta G_{CS} = -RT\ln k$ for equilibrium conditions in Equation (4).

[31] Spectroscopically, the 20 nm difference between the two oxidized species, that is, $(exTTF)_1^{\bullet+}$ and $(exTTF)_2^{\bullet+}$ opened the possibility for us to successfully analyze the charge-shift rates, by following the band grow in at 660 nm. The rate constants are $7.7 \times 10^8\ s^{-1}$ (toluene), $8.2 \times 10^8\ s^{-1}$ (THF), $9.3 \times 10^8\ s^{-1}$ (benzonitrile) and $1.2 \times 10^9\ s^{-1}$ (DMF).

[32] Further support for this assumption comes from the very slow charge recombination rate under barrier-less conditions $3.4 \times 10^7\ s^{-1}$, as derived from the intercept of the Arrhenius plot (see Figure 10). Therefore, the only reasonable rationale for this trend implies a sequential electron transfer ([Eq. (5)]), that is a thermally activated process, via the intermediate $C_{60}^{\bullet-}$-$(exTTF)_1^{\bullet+}$-$(exTTF)_2$ rather than electron tunneling by means of superexchange ([Eq. (6)]).

[33] The smaller energy gap in triad **25** (0.06 eV) expedites the charge recombination.

Received: October 10, 2002
Revised: December 16, 2002 [F4494]